



Effect of Different Amounts of TiF_3 on the Reversible Hydrogen Storage Properties of $2\text{LiBH}_4\text{-Li}_3\text{AlH}_6$ Composite

Yun Li^{1,2}, Yuxian Zhang^{1*} and Lixin Chen²

¹School of Mechanical and Electrical Engineering, Quzhou College of Technology, Quzhou, China, ²School of Materials Science and Engineering, Zhejiang University, Hangzhou, China

OPEN ACCESS

Edited by:

Feng Luo,
East China University of Technology,
China

Reviewed by:

Haizhen Liu,
Guangxi University, China
Tomasz Czujko,
Military University of Technology in
Warsaw, Poland

*Correspondence:

Yuxian Zhang
zyx@qzct.net

Specialty section:

This article was submitted to
Inorganic Chemistry,
a section of the journal
Frontiers in Chemistry

Received: 10 April 2021

Accepted: 03 May 2021

Published: 14 May 2021

Citation:

Li Y, Zhang Y and Chen L (2021) Effect of Different Amounts of TiF_3 on the Reversible Hydrogen Storage Properties of $2\text{LiBH}_4\text{-Li}_3\text{AlH}_6$ Composite. *Front. Chem.* 9:693302. doi: 10.3389/fchem.2021.693302

Hydrogen is a potential green alternative to conventional energy carriers such as oil and coal. Compared with the storage of hydrogen in gaseous or liquid phases, the chemical storage of hydrogen in solid complex hydrides is safer and more effective. In this study, the complex hydride composite $2\text{LiBH}_4\text{-Li}_3\text{AlH}_6$ with different amounts of TiF_3 was prepared by simple ball-milling and its hydrogen storage properties were investigated. Temperature programmed desorption and differential scanning calorimetry were used to characterize the de/rehydrogenation performance, and X-ray diffraction and scanning electron microscopy (SEM) were used to explore the phase structure and surface topography of the materials. The dehydrogenation temperature decreased by 48°C in $2\text{LiBH}_4\text{-Li}_3\text{AlH}_6$ with 15 wt% TiF_3 composites compared to the composite without additives while the reaction kinetics was accelerated by 20%. In addition, the influence of hydrogen back pressure on the $2\text{LiBH}_4\text{-Li}_3\text{AlH}_6$ with 5 wt% TiF_3 composite was also investigated. The results show that hydrogen back pressure between 2.5 and 3.5 bar can improve the reversible performance of the composite to some extent. With a back pressure of 3.5 bar, the second dehydrogenation capacity increased to 4.6 wt% from the 3.3 wt% in the $2\text{LiBH}_4\text{-Li}_3\text{AlH}_6$ composite without hydrogen back pressure. However, the dehydrogenation kinetics was hindered. About 150 h, which is 100 times the time required without back pressure, was needed to release 8.7 wt% of hydrogen at 3.5 bar hydrogen back pressure. The SEM results show that aluminum was aggregated after the second cycle of dehydrogenation at the hydrogen back pressure of 3 bar, resulting in the partial reversibility of the 5 wt% TiF_3 -added $2\text{LiBH}_4\text{-Li}_3\text{AlH}_6$ composite.

Keywords: $2\text{LiBH}_4\text{-Li}_3\text{AlH}_6$, hydrogen storage performance, catalytic modification, hydrogen back pressure, reversible performance

INTRODUCTION

As a new energy source, hydrogen has great potential to solve the serious energy depletion and atmospheric pollution caused by excessive utilization of conventional energy sources. Hydrogen is the most abundant element in the Universe. The calorific value of 1 kg of hydrogen is 140 megajoules of energy, which is three times of that of the amount of energy released by the same weight of oil.

Moreover, water vapor is the only combustion product of hydrogen, making it a pollution-free energy source. However, the limitations of hydrogen storage technology have hindered its practical application.

As a promising candidate for solid-state hydrogen storage, LiBH_4 has a high theoretical gravimetric hydrogen density of 18.5 wt%, which is the highest among all the solid hydride materials. (Züttel et al., 2003) first studied the desorption properties of LiBH_4 . The material released 0.3 wt% hydrogen at 200°C and 1 wt% hydrogen at 320°C. After heating to 500°C, rapid hydrogen desorption was observed, and 9 wt% of hydrogen was released. This capacity meets the requirements of the US Department of Energy (DOE) (Jain et al., 2010), but the desorption temperature is too high for practical applications, and the dehydrogenation kinetics also need to be improved.

Many researchers have focused on the modification of LiBH_4 using various methods, such as composite modification (Xia et al., 2011; Langmi et al., 2012; Bilen et al., 2015; Liu et al., 2015; Sofianos et al., 2017), catalyst modification (Puszkiewski et al., 2014; Ma et al., 2016; Zhang et al., 2018), and nanoengineering (Zhao et al., 2014; Surrey et al., 2016; Sofianos et al., 2018). Compositing LiBH_4 with other active hydrides is an effective way to enhance its hydrogen storage performance. For example, Liu et al., 2016 milled LiBH_4 with AlH_3 to form a $2\text{LiBH}_4 + \text{AlH}_3$ composite. The dehydrogenation temperature of the $2\text{LiBH}_4 + \text{AlH}_3$ composite was reduced by 30°C compared with pure LiBH_4 , and 11.2 wt% hydrogen was obtained. (Ding et al. 2019) found that in a nano-sized composite of LiBH_4 and MgH_2 prepared by ball-milling with aerosol spraying (BMAS), the LiBH_4 released hydrogen at 265°C, and approximately 5.0 wt% H_2 was reversible in the first five dehydrogenation and rehydrogenation cycles. Using the shrinking-core model, it was found that a larger interfacial area between LiBH_4 and MgH_2 improves the dynamics of the nano $2\text{LiBH}_4 + \text{MgH}_2$ mixture (Ding et al., 2019).

Other researchers have prepared binary (Mao et al., 2009b; Yu et al., 2010; Hansen et al., 2013; Li et al., 2013; Mustafa et al., 2018; Yahya et al., 2019) or ternary (Yang et al., 2012; Liu et al., 2021) composite systems of LiBH_4 and other complex hydrides (Halim Yap et al., 2018; Halim Yap and Ismail, 2018), such as $\text{LiBH}_4\text{-LiAlH}_4$ (Thaweelap and Utke, 2016; Meethom et al., 2020), $\text{LiBH}_4\text{-Li}_3\text{AlH}_6$ (Choi et al., 2011b), $\text{LiBH}_4\text{-NaBH}_4$ (Dematteis et al., 2016), $\text{LiBH}_4\text{-NaAlH}_4$, $\text{LiBH}_4\text{-Mg}(\text{BH}_4)_2$ (Zheng et al., 2020), $\text{LiBH}_4\text{-Ca}(\text{BH}_4)_2$ (Ampoumogli et al., 2015), $\text{LiBH}_4\text{-Mg}_2\text{NiH}_4$ (Bergemann et al., 2019), $\text{LiBH}_4\text{-NaBH}_4\text{-MgH}_2$ (Xiang et al., 2018), and $\text{LiBH}_4\text{-Li}_3\text{AlH}_6\text{-MgH}_2$ (Lin et al., 2020). Bergeman et al. (Bergemann, et al. 2019) investigated the reaction mechanism of a $\text{LiBH}_4\text{-Mg}_2\text{NiH}_4$ composite. They found that the dehydrogenation path was significantly influenced by the back pressure and temperature. When the back pressure was increased to 50 bar, Mg_2NiH_4 reacted with solid LiBH_4 below 270°C, and the reaction enthalpy was reduced by 13 kJ/mol H_2 . In Thaweelap's work (Thaweelap and Utke, 2016), LiBH_4 and LiAlH_4 were synthesized together with Ti-based catalysts or carbon nanotubes to achieve a synergistic effect between the catalysts and composites. Both the kinetics and thermodynamics of the samples were improved. In addition, the reversibility of the

$\text{LiBH}_4\text{-LiAlH}_4\text{-MWCNT}$ composite was increased to 3.7 wt% in the second cycle compared to 2.8 wt% in the $\text{LiBH}_4\text{-LiAlH}_4$ composite. Wu (Wu et al. 2012) revealed the reaction mechanism of a $\text{LiBH}_4\text{-Li}_3\text{AlH}_6$ composite, which received 8.5 wt% hydrogen in the dehydrogenation process. Zhou (Zhou et al. 2017) prepared a $2\text{LiBH}_4\text{-LiAlH}_4$ composite nanoconfined in an RFC aerogel, and found that both the thermodynamic and kinetic properties were enhanced.

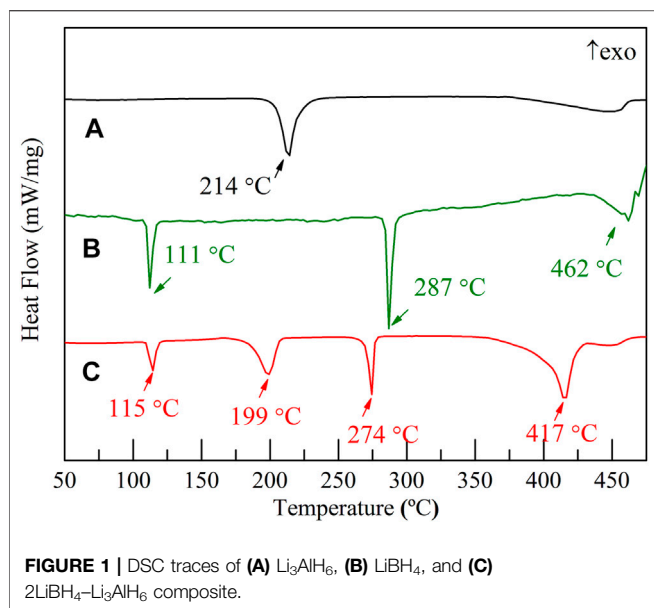
Some catalysts such as CaH_2 (Jiang et al., 2012), NbF_5 (Mao et al., 2013), TiF_3 (Mao et al., 2010) and NbCl_5 (Tu et al., 2015) destabilize LiBH_4 to decompose H_2 under moderate conditions. Ming mixed LiBH_4 with several additives using the ball-milling method (Au and Jurgensen, 2006). The modified mixtures desorbed hydrogen at a lower temperature and higher rate. Among the various additives, Ti-based catalysts had an obvious effect. Choi (Choi et al. 2011a) demonstrated that TiCl_3 could promote desorption in a $\text{Li}_3\text{AlH}_6/2\text{LiBH}_4$ composite at a lower temperature. Because of the catalyst effect of TiCl_3 , Li_3AlH_6 started to release hydrogen at 81°C, and LiBH_4 released hydrogen at 226°C, which are 130 and 200°C lower than the temperatures at which hydrogen was released by pure Li_3AlH_6 and LiBH_4 , respectively. A novel two-dimensional (2D) layered Ti_3C_2 material was added to the $\text{LiBH}_4\text{-THF}$ solution to synthesize a series of $\text{LiBH}_4\text{-}\chi\text{Ti}_3\text{C}_2$ composites with different mass ratios. The $\text{LiBH}_4\text{-}2\text{Ti}_3\text{C}_2$ composite released hydrogen at 172.6°C, and its activation energy was reduced by 50% compared to that of pure LiBH_4 (Zang et al., 2018). TiF_3 is a well known catalyst for solid-state hydrogen storage materials. It effectively improved the hydrogen storage performance of $\text{LiAlH}_4\text{-MgH}_2$ (Mao et al., 2011), $\text{MgH}_2\text{-NaAlH}_4$ (Ismail et al., 2012) and $2\text{NaAlH}_4\text{-Ca}(\text{BH}_4)_2$ (Mustafa and ismail, 2019) binary composite.

In this study, a ternary composite of $2\text{LiBH}_4\text{-Li}_3\text{AlH}_6$ with different amounts of TiF_3 (the mass percent of TiF_3 were 5, 10, and, 15%) was prepared by a high-energy ball milling method. The synergistic effects between the composite and the catalyst were investigated together with the influence of the hydrogen back pressure on the reversibility.

MATERIALS AND METHODS

LiBH_4 powder (95% purity) and TiF_3 powder (99% purity) were purchased from Acros Organics and Sigma Aldrich, respectively. Li_3AlH_6 powder was obtained by mixing LiAlH_4 (95% purity, Sigma Aldrich) and LiH (98% purity, Alfa Aesar) using a high-energy ball-milling method at a ball-to-powder ratio of 40:1 (Li et al., 2020). All the materials used in this work were stored in a glove box purchased from Mikrouna. The glove box was filled with high-purity argon to purge the atmosphere, and the water vapor content was less than 1 ppm. The $2\text{LiBH}_4\text{-Li}_3\text{AlH}_6$ series with and without TiF_3 composites was weighed and mixed in this glove box, and then loaded in a sealed stainless ball-milling tank. Planetary ball-milling equipment (QM-3SP4) was used to grind the materials at 300 revolutions per minute for 1 h.

A Sievert-type instrument which recorded the pressure change of the hydrogen released during the heating process was used to



evaluate the dehydrogenation/rehydrogenation performance of the materials. Approximately 200 mg of each sample was charged into a thin stainless-steel tube reactor. The reactor was then heated from ambient temperature to the set temperature at a constant heating rate. The time, temperature, and pressure data were recorded every ten seconds. The amount of hydrogen released or absorbed during the heating process was calculated using the ideal gas state equation. Differential scanning calorimetry (DSC, Netzsch STA 449F3/Netzsch Q403C) was used to evaluate the thermal effects of the materials. In the glove box, about 1–1.5 mg of samples were loaded each time and sealed in an aluminum crucible. Both the sample crucible and the reference crucible were placed in the reaction chamber of the DSC equipment, which was filled with flowing high purity argon at a flow rate of 50 ml/min.

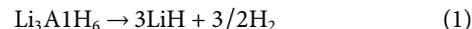
X-ray diffraction (XRD, X'Pert-PRO) and scanning electron microscopy (SEM, FEI FSEM SIRION-100) were used to analyze the phase structure and observe the surface topography of the material. The XRD K-Alpha1 and K-Alpha2 wavelengths were 1.540598 Å and 1.544426 Å, respectively. The samples were sealed in a transparent macromolecular container to prevent oxidation. Fourier transform infrared spectroscopy (FT-IR, Bruker, Tensor 27) at the scan rate of $30\text{ cm}^{-1}/\text{min}$ and resolution of 0.5 cm^{-1} was used for chemical bond analysis. The crucibles used in the experiments were aluminum crucibles.

RESULTS AND DISCUSSION

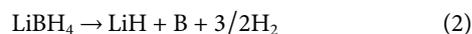
DSC Traces of LiBH_4 , Li_3AlH_6 , and $\text{LiBH}_4\text{-Li}_3\text{AlH}_6$ Samples

The DSC traces of the Li_3AlH_6 , LiBH_4 , and $2\text{LiBH}_4\text{-Li}_3\text{AlH}_6$ samples at the heating rate of $5^\circ\text{C}/\text{min}$ from ambient temperature to 500°C are shown in **Figure 1**. In the Li_3AlH_6 sample (**Figure 1A**), there is an endothermic peak at 214°C due to the

decomposition process of Li_3AlH_6 . The last peak in the DSC trace of Li_3AlH_6 was the decomposition of LiH (Aresfernandez, 2007). The decomposition reaction of Li_3AlH_6 and the resulting products are described by **Eq. 1** (Zang, et al., 2018):



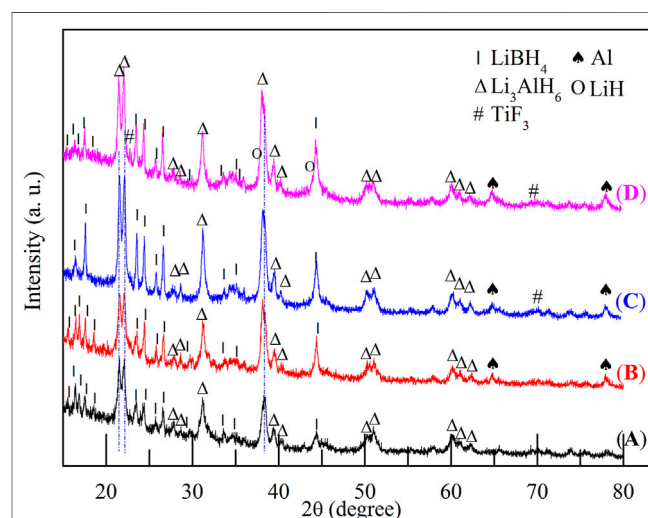
There are three endothermic peaks in the DSC trace of LiBH_4 shown in **Figure 1B**. The first peak at 111°C is the lattice transition peak of LiBH_4 , and the second peak at 287°C corresponds to the melting of LiBH_4 (Züttel, et al., 2003). The third peak is wider than the first two and indicates the decomposition of LiBH_4 (Li et al., 2017). The decomposition process is shown in **Eq. 2** (Mao et al., 2009a):

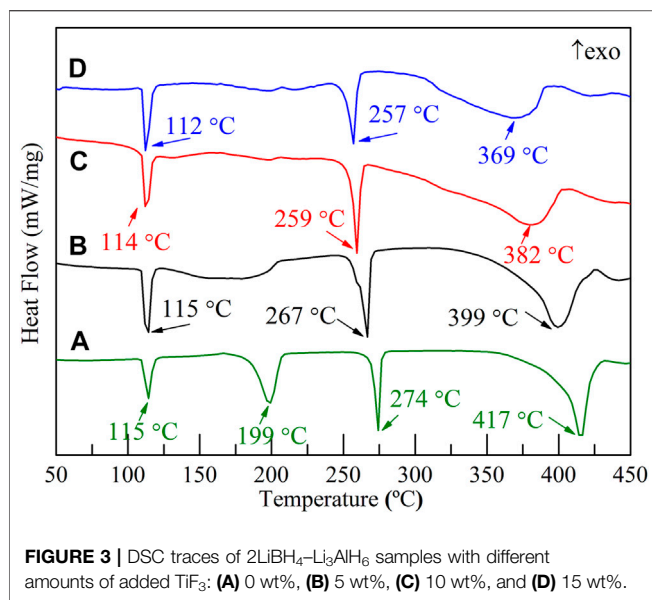


Four endothermal peaks corresponding to the characteristic peaks of the components were observed for the $2\text{LiBH}_4\text{-Li}_3\text{AlH}_6$ composite. The LiBH_4 in the $2\text{LiBH}_4\text{-Li}_3\text{AlH}_6$ composite melted at 274°C , which is 13°C lower than the melting point of pure LiBH_4 . The second and the fourth endothermal peaks mean a rapid dehydrogenation temperature of Li_3AlH_6 and LiBH_4 , were 199 and 417°C (see **Figure 1C**), which were lower than pure Li_3AlH_6 and LiBH_4 , indicating that the dehydrogenation performance of the $2\text{LiBH}_4\text{-Li}_3\text{AlH}_6$ composite obtained a better thermal performance.

Influence of TiF_3 on Hydrogen Desorption Performance of $2\text{LiBH}_4\text{-Li}_3\text{AlH}_6$ Composite

The hydrogen storage properties of the $2\text{LiBH}_4\text{-Li}_3\text{AlH}_6$ composite both in its original state and in the presence of TiF_3 were investigated in this study. The samples were weighed and loaded in a glove box filled with pure argon. The

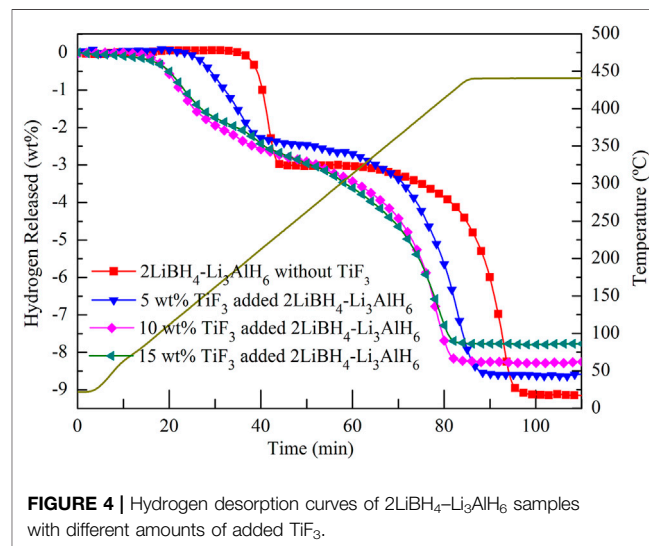




mass percentages of TiF₃ in the four samples were 0, 5, 10, and 15 wt%. All the samples were prepared by ball-milling for 1 h, and XRD was used to determine the composition of the samples. LiBH₄ and Li₃AlH₆ peaks were observed in the 2LiBH₄-Li₃AlH₆ sample without the TiF₃ additive (Figure 2A). The main diffraction peaks of the three 2LiBH₄-Li₃AlH₆ composites with different amount of TiF₃ (Figures 2B–D) correspond to those of the 2LiBH₄-Li₃AlH₆ sample without additive. The weak diffraction peaks at 23° or 70° in Figure 2C and Figure 2D could be attributed to TiF₃. The absence of a TiF₃ peak in Figure 2B may possibly be due to the small amount of highly dispersed TiF₃. As the TiF₃ content increased, the diffraction peak of Al in the 2LiBH₄-Li₃AlH₆ with TiF₃ composites gradually became obvious, and weak LiH peaks appeared at 38° and 44°. These results indicate that TiF₃ destabilized Li₃AlH₆ by promoting its decomposition into LiH and Al during the ball-milling process (Ares, 2008). Approximately 1 mg of the prepared samples was loaded into an aluminum oxide crucible for the DSC test each time. The results are shown in Figure 3. Comparing the 2LiBH₄-Li₃AlH₆ samples with TiF₃ (Figures 3B–D) or without TiF₃ (Figure 3A), the lattice transition peaks of LiBH₄, which were between 112 and 115°C, were almost unchanged. The melting peak of LiBH₄ decreased from 274 to 257°C as the amount of TiF₃ increased. In addition, compared with the 2LiBH₄-Li₃AlH₆ sample, the Li₃AlH₆ decomposition peak shifted obviously to lower temperatures and became wider in the 2LiBH₄-Li₃AlH₆ with 5 wt% TiF₃. In the samples with 10 and 15 wt% TiF₃, the typical endothermic peak of Li₃AlH₆ was almost undetectable. A possible reason for this is the partial decomposition of Li₃AlH₆ during the ball-milling process (Liu, 2010). This result is consistent with the XRD patterns (Figure 2), in which LiH and Al were detected in the TiF₃-added ball-milling samples, and indicates that TiF₃ is an effective catalyst that can destabilize Li₃AlH₆ at a lower temperature. LiBH₄ decomposed at 399, 382, and 369°C in the 2LiBH₄-Li₃AlH₆ composite with 5, 10, and 15 wt% TiF₃ additives, respectively. Faster dehydrogenation

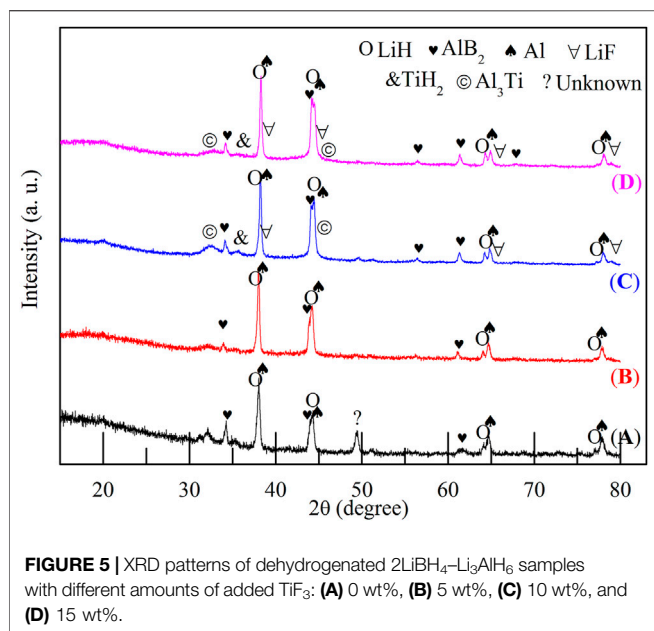
TABLE 1 | Theoretical hydrogen storage capacity and actual hydrogen desorption capacity of 2LiBH₄-Li₃AlH₆ samples with different amounts of TiF₃.

TiF ₃ content (wt%)	0	5	10	15
Theoretical hydrogen storage capacity (wt%)	9.24	8.77	8.31	7.85
Actual hydrogen desorption capacity (wt%)	9.15	8.67	8.27	7.71



kinetics were also obtained as the dehydrogenation peak of LiBH₄ became broader with the increase in the amount of TiF₃ (Zang, et al., 2018). The introduction of the TiF₃ catalyst promoted both the thermal decomposition and the kinetic properties of LiBH₄ and Li₃AlH₆.

A temperature-programmed desorption (TPD) test was performed to study the dehydrogenation properties with and without TiF₃ in the 2LiBH₄-Li₃AlH₆ samples. Table 1 shows the theoretical hydrogen storage capacities of the 2LiBH₄-Li₃AlH₆ samples with different amounts of TiF₃. As the amount of TiF₃ increased, the weight percentage of H in 1 g of ball-milled sample decreased from 9.24 wt% to 7.85 wt%, as shown in Table 1. Approximately 200 mg of each sample was loaded into a stainless-steel reactor. The reactor was heated from room temperature to 440°C at a heating rate of 5°C/min and maintained at 440°C for half an hour. The hydrogen desorption curves of the four samples are shown in Figure 4. The 2LiBH₄-Li₃AlH₆ sample underwent a two-step dehydrogenation process in which the release of hydrogen began at 190°C and approximately 3 wt% of hydrogen was released in the first step. The second step began at approximately 330°C and the remaining 6.15 wt% of hydrogen was released. The total dehydrogenation capacity of 9.15 wt% is consistent with the theoretical hydrogen storage capacity. In the 2LiBH₄-Li₃AlH₆ with 5 wt% TiF₃ composite, the initial dehydrogenation temperatures of the two-step process decreased to 110 and 270°C. As the amount of TiF₃ increased, the decomposition temperatures of Li₃AlH₆ and LiBH₄ tended to



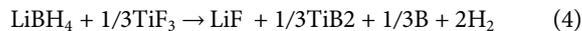
decrease. The Li₃AlH₆ decomposed at 88°C in the 10 wt% TiF₃-added 2LiBH₄-Li₃AlH₆ composite, compared to 85°C in the 15 wt% TiF₃-added sample. LiBH₄ started to release hydrogen at 238°C in the 10 wt% TiF₃-added sample and at 225°C in the 15 wt% TiF₃-added sample. These results indicate that the addition of TiF₃ improved the thermodynamic properties of the 2LiBH₄-Li₃AlH₆ composites. In contrast to the 2LiBH₄-Li₃AlH₆ composite, the absence of a “platform area” between the first and second steps of the composites with TiF₃ indicated that LiBH₄ tended to decompose at a lower temperature and the rate of hydrogen desorption were accelerated by the catalytic effect of TiF₃. The time required for total decomposition decreased to 82 min when the TiF₃ amount was 15 wt% compared to the 95 min required for the 2LiBH₄-Li₃AlH₆ composite without TiF₃. Clearly, the addition of TiF₃ enhanced both the thermodynamic and kinetic properties of the 2LiBH₄-Li₃AlH₆ composite system. However, the theoretical hydrogen storage capacity and the actual hydrogen desorption capacity of the composites with TiF₃ decreased as the amount of TiF₃ increased (shown in **Table 1**).

To reveal the dehydrogenation pathway and catalytic effect of TiF₃, the XRD patterns of the dehydrogenation products of the four samples are displayed in **Figure 5**. In the 2LiBH₄-Li₃AlH₆ composite (**Figure 5A**), the presence of LiH, Al, and AlB₂ phases indicates that LiBH₄ reacted with Al generated from Li₃AlH₆ (Li et al., 2020) *in situ* to form AlB₂, as shown in **Eq. 3** (Choi et al., 2011b; Soru, 2014; Meethom, et al. 2020):



The unknown peak near 49° was also observed in previous studies (Mao et al., 2009a; Li, 2012). This peak was probably due to an intermediate dehydrogenation product of LiBH₄ and Li₃AlH₆. In the samples with 10 wt% TiF₃ (**Figure 5C**) and the 15 wt% TiF₃ (**Figure 5D**), some Ti-based or F-based phases could be detected

in addition to the peaks corresponding to LiH, Al, and AlB₂. The LiF characteristic peaks near 38° and 79° correspond to the reaction products between LiBH₄ and TiF₃, as shown in **Eq. 4** (Mao et al., 2009b; Guo, 2010).

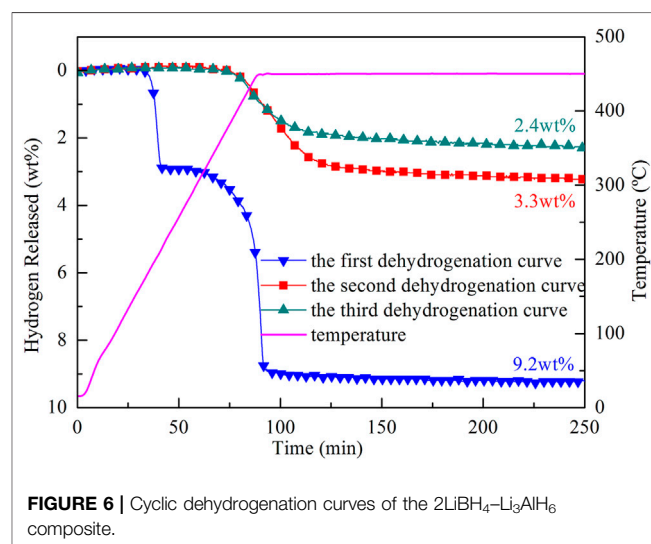


The TiH₂ peaks at 36° and Al₃Ti peaks at 31° and 44° may possibly be due to reaction products between Li₃AlH₆ and TiF₃, the reaction mechanisms of which were explored in Liu’s work (Liu et al., 2010). The diffraction peak of AlB₂ appeared at 57° in the 10 and 15 wt% TiF₃-added samples, indicating that the amount of AlB₂ was increased.

Reversible Performance of TiF₃ Added 2LiBH₄-Li₃AlH₆ Composite with Different Back Pressures

The reversible performance of the 2LiBH₄-Li₃AlH₆ composite was investigated in this study. Approximately 200 mg samples of 2LiBH₄-Li₃AlH₆ composite were loaded in a tubular reactor and heated to 450°C at a heating rate of 5°C/min. The dehydrogenated samples were maintained at 450°C for 250 min and then cooled down to ambient temperature naturally. The hydrogen adsorption process was performed at the hydrogen pressure of 100 bar at 450°C for 10 h. The dehydrogenation curves of the 2LiBH₄-Li₃AlH₆ composite are shown in **Figure 6**. The hydrogen release capacity of the 2LiBH₄-Li₃AlH₆ composite was 9.2 wt% in the first cycle, and 3.3 wt% and 2.4 wt% in the second and third cycles, respectively. Unlike the two-step desorption reactions of the first cycle, only one-step reactions occurred in the second and third cycles, and the initial dehydrogenation temperature reached as high as 400°C.

The observation of the B-H bond of LiBH₄ at 2,200–2,400 cm⁻¹ in the FT-IR curves of the ball-milled sample and the resorption sample (**Figure 7**) indicates that the 2LiBH₄-Li₃AlH₆ composite was partially reversible, and that the



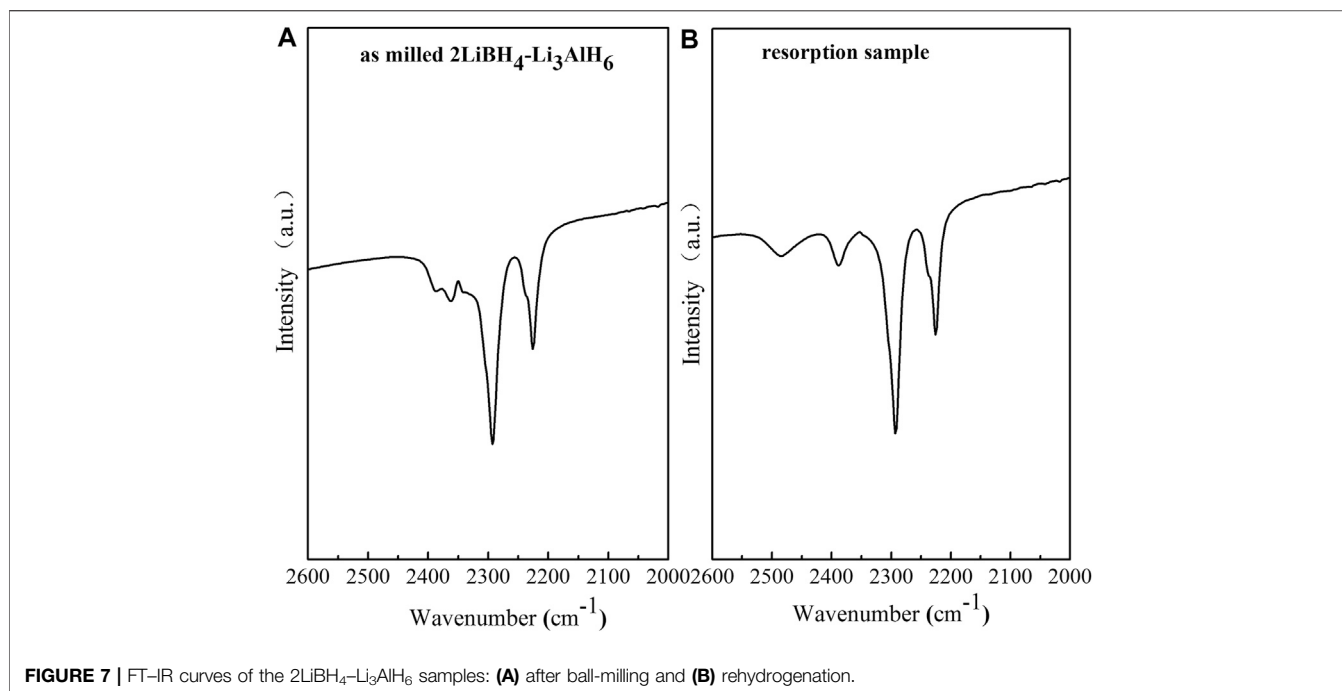


FIGURE 7 | FT-IR curves of the $2\text{LiBH}_4\text{-Li}_3\text{AlH}_6$ samples: **(A)** after ball-milling and **(B)** rehydrogenation.

reversible component was LiBH_4 . The formation process of LiBH_4 is given by Eq. 5 (Li et al., 2012):

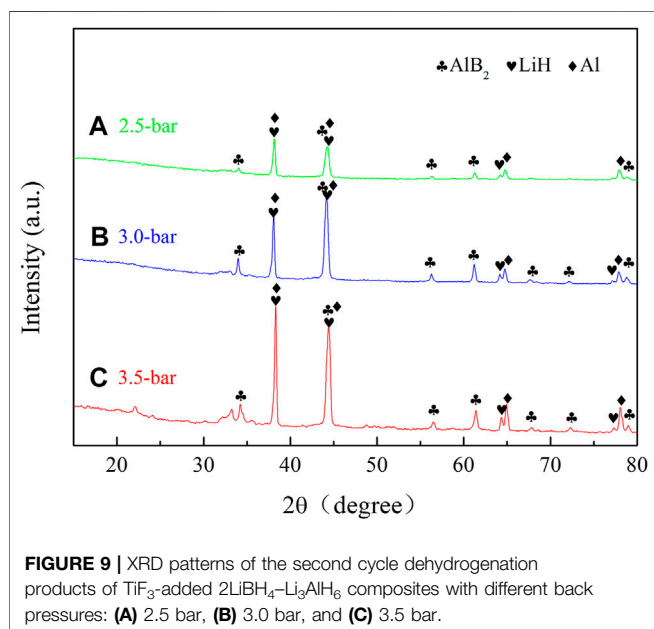
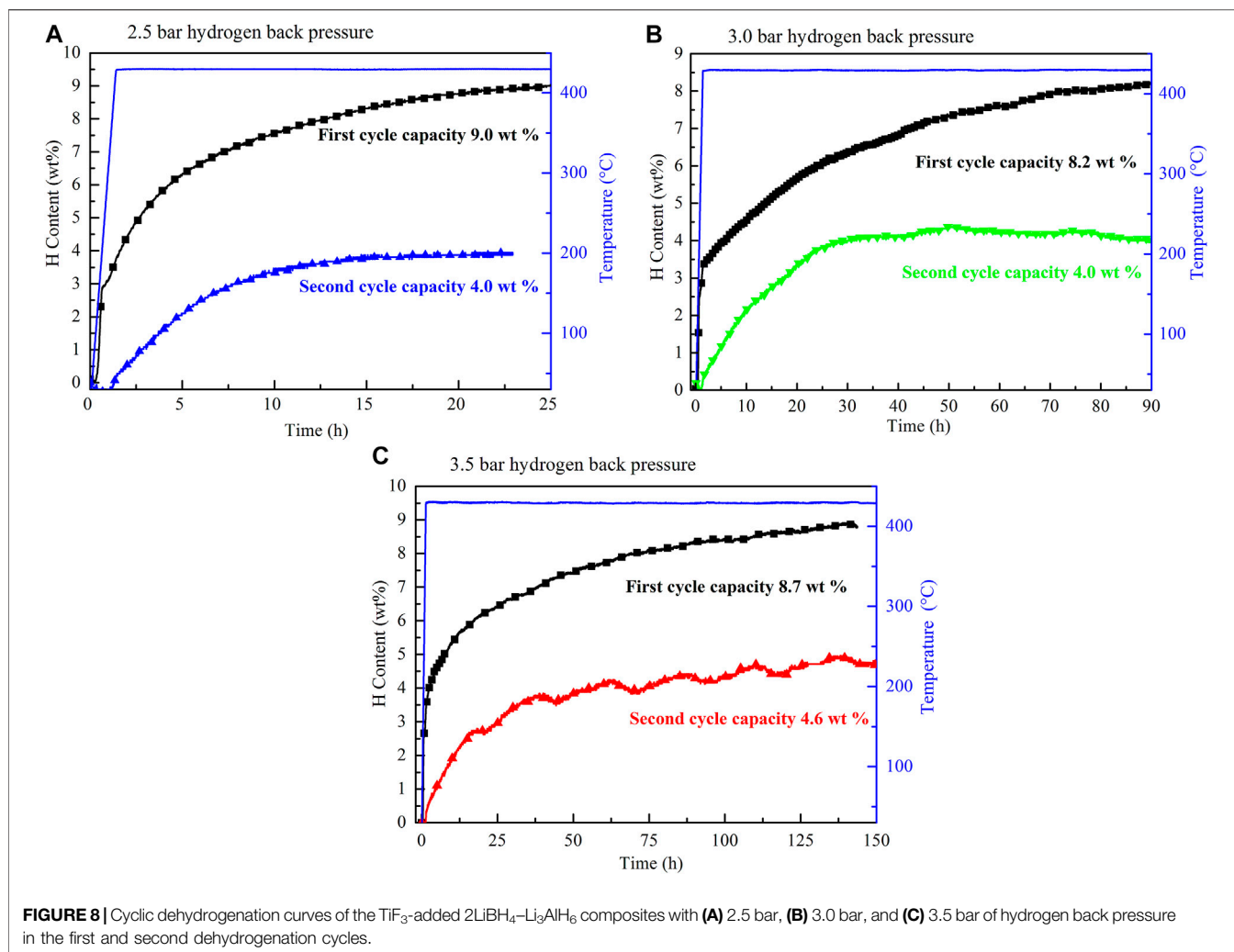


In the second and third dehydrogenation cycles, the hydrogen releasing capacities were lower than 3.5 wt%, which is significantly lower than the first one. Therefore, further research is required to improve the reversible performance. In a previous work, Mao (Mao et al., 2013) reported that hydrogen back pressure could improve the cyclic performance of LiBH_4 -based composites. As mentioned earlier, TiF_3 is a superior catalyst for improving the hydrogen storage performance of the $2\text{LiBH}_4\text{-Li}_3\text{AlH}_6$ composite. Therefore, the studies that follow focus on the influence of hydrogen back pressure on the dehydrogenation and cyclic performance of TiF_3 -added $2\text{LiBH}_4\text{-Li}_3\text{AlH}_6$ composites. The $2\text{LiBH}_4\text{-Li}_3\text{AlH}_6$ with 5 wt% TiF_3 composite was dehydrogenated at 425°C with initial hydrogen back pressures of 2.5, 3.0, and, 3.5 bar. The dehydrogenated samples then began to absorb hydrogen at 100 bar hydrogen pressure for 10 h. The dehydrogenation curves at different hydrogen back pressures in the first and second cycles are shown in Figure 8. The dehydrogenation capacity in the first cycle at the different hydrogen back pressures was about 8.2 wt% to 9.0 wt% in the $2\text{LiBH}_4\text{-Li}_3\text{AlH}_6$ with 5 wt% TiF_3 composite, which is lower than its theoretical capacity. In the second dehydrogenation cycle, the amount of hydrogen released was 4.0 wt% or 4.6 wt%, which are higher than that of $2\text{LiBH}_4\text{-Li}_3\text{AlH}_6$ composite (3.3 wt%). From these results, it could be concluded that a hydrogen back pressure of

between 2.5 and 3.5 bar and the addition of TiF_3 could improve the reversible performance of the $2\text{LiBH}_4\text{-Li}_3\text{AlH}_6$ composite to some extent. However, the dehydrogenation kinetics of the $2\text{LiBH}_4\text{-Li}_3\text{AlH}_6$ with TiF_3 composite was hindered by the hydrogen back pressure. It took more than 150 h to release 8.7 wt% hydrogen with 3.5 bar hydrogen back pressure in the TiF_3 -added $2\text{LiBH}_4\text{-Li}_3\text{AlH}_6$ composite, compared to 1.5 h in the composite without back pressure.

The XRD patterns of the second-cycle dehydrogenation products are shown in Figure 9. Three phases, namely, AlB_2 , LiH , and Al , were detected in all the curves. Compared with Figure 5B, the diffraction intensity of AlB_2 increased in Figures 9A–C, which resulted in the improved reversible performance.

The surface topography of the $2\text{LiBH}_4\text{-Li}_3\text{AlH}_6$ composites under different conditions was observed by SEM. The ball-milled sample (Figure 10A) displayed a coral-like structure. At $50,000\times$ magnification (inset of Figure 10A), the particles had a rod-shaped appearance with a length of approximately $3\ \mu\text{m}$ and a width of $1\ \mu\text{m}$. After the first cycle of dehydrogenation, the particles agglomerated into aggregates (Figure 10B) instead of rod-shaped structures. After the second cycle of dehydrogenation at the back pressure of 3 bar, some spherical particles were formed, as shown in Figure 10C. Using the energy dispersive spectrometer, these particles were found to consist of metallic aluminum. The aggregation and growth of metallic aluminum led to a poor dispersion and reduced active surface area of the dehydrogenation products, which may explain the partial reversibility of the $2\text{LiBH}_4\text{-Li}_3\text{AlH}_6$ composites (Meethom et al., 2020).



CONCLUSION

In this study, the dehydrogenation performance and influence of back pressure on the $2\text{LiBH}_4\text{-Li}_3\text{AlH}_6$ with/without TiF_3 composites were investigated. TiF_3 enabled Li_3AlH_6 and LiBH_4 to desorb hydrogen at lower temperatures. With an increase in the amount of TiF_3 , the dehydrogenation temperature decreased significantly. In the 15% TiF_3 -added composite, Li_3AlH_6 decomposed at 85°C and LiBH_4 at 225°C , that is, at 105°C lower for each component compared with the undoped sample. However, when the TiF_3 content was increased to 15 wt%, the hydrogen capacity of the composite was reduced to 7.85 wt%, which is 15% lower than that without the $2\text{LiBH}_4\text{-Li}_3\text{AlH}_6$ composite. In the reversibility evaluation, the hydrogen back pressures of 2.5 bar, 3.0 bar, and 3.5 bar hydrogen were adopted. The results indicate that the back pressure could enhance the reversible performance of $2\text{LiBH}_4\text{-Li}_3\text{AlH}_6$ composite to some extent. A reversible hydrogen capacity of 4.6 wt% was obtained with a back pressure of 3.5 bar in the TiF_3 -added $2\text{LiBH}_4\text{-Li}_3\text{AlH}_6$ composites. However, the kinetics of the TiF_3 -added $2\text{LiBH}_4\text{-Li}_3\text{AlH}_6$ composites were hindered. More

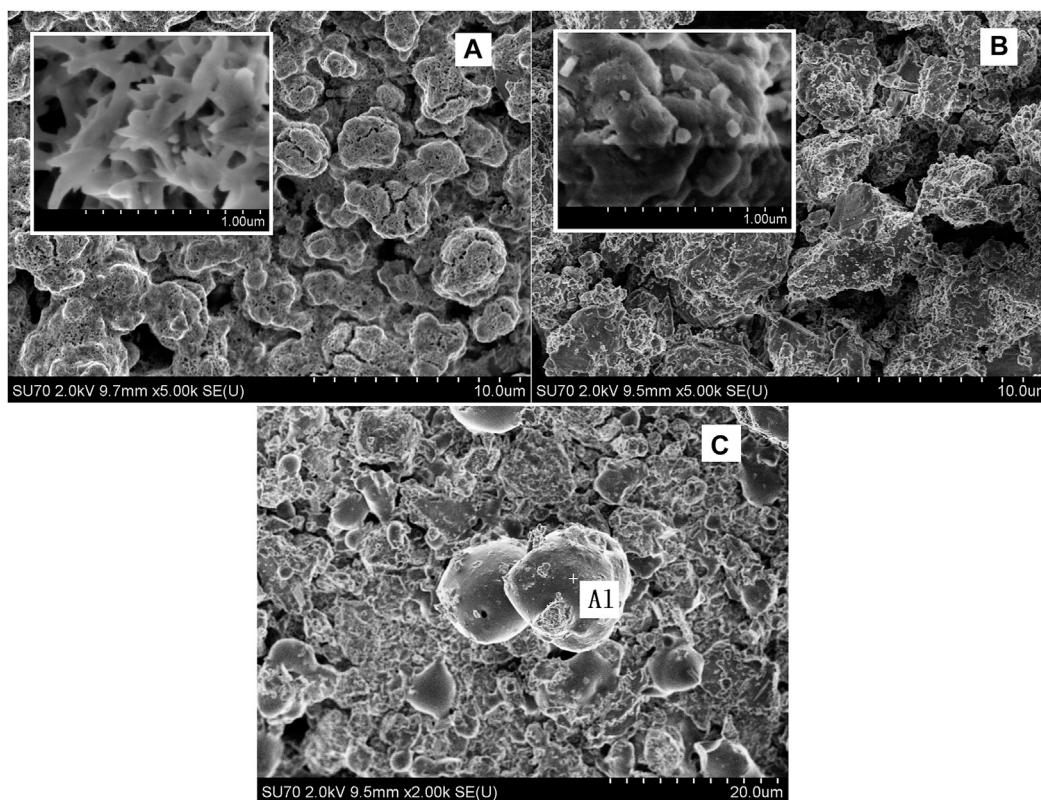


FIGURE 10 | SEM images of the $2\text{LiBH}_4\text{-Li}_3\text{AlH}_6$ composites: **(A)** ball-milled sample, **(B)** sample after first dehydrogenation cycle, and **(C)** sample after second dehydrogenation cycle with 3 bar back pressure.

than 150 h were required to complete the hydrogen release process at the hydrogen back pressure of 3.5 bar. The SEM results showed that metallic aluminum was aggregated, resulting in poor dispersion of the dehydrogenated phases and reduced active surface area. Further research is needed to improve the desorption and absorption performance of LiBH_4 .

DATA AVAILABILITY STATEMENT

The original contributions presented in the study are included in the article/Supplementary Material, further inquiries can be directed to the corresponding author.

AUTHOR CONTRIBUTIONS

YL and LC: conception and design of study. YL and YZ: acquisition of data. YL analysis and/or interpretation of data.

REFERENCES

Ampoumogli, A., Charalambopoulou, G., Javadian, P., Richter, B., Jensen, T. R., and Steriotis, T. (2015). Hydrogen Desorption and Cycling Properties of

YL: drafting the manuscript. YZ and LC revising the manuscript critically for important intellectual content. YL, YZ, and LC approval of the version of the manuscript to be published.

FUNDING

This work was supported by the National Natural Science Foundation of China (51671173), the Quzhou Science and Technology Guidance Project (2020012) and the Zhejiang Province Education Department Project (FG2020220). The authors would like to acknowledge these funds for their support.

ACKNOWLEDGMENTS

We would like to thank Editage (www.editage.com) for English language editing.

Composites Based on Mesoporous Carbons and a $\text{LiBH}_4\text{-Ca}(\text{BH}_4)_2$ Eutectic Mixture. *J. Alloys Comp.* 645, S480–S484. doi:10.1016/j.jallcom.2014.12.077
Ares, J. R., Aguey-Zinsou, K.-F., Porcu, M., Sykes, J. M., Dornheim, M., Klassen, T., et al. (2008). Thermal and Mechanically Activated Decomposition of LiAlH_4 . *Mater. Res. Bull.* 43 (5), 1263–1275. doi:10.1016/j.materresbull.2007.05.018

- Aresfernandez, J., Agueyzinsou, F., Elsaesser, M., Ma, X., Dornheim, M., Klassen, T., et al. (2007). Mechanical and Thermal Decomposition of $\text{LiAlH}_4\text{LiAlH}_4$ with Metal Halides. *Int. J. Hydrogen Energ.* 32 (8), 1033–1040. doi:10.1016/j.ijhydene.2006.07.011
- Au, M., and Jurgensen, A. (2006). Modified Lithium Borohydrides for Reversible Hydrogen Storage. *J. Phys. Chem. B* 110 (13), 7062–7067. doi:10.1021/jp0562400
- Bergemann, N., Pistidda, C., Uptmoor, M., Milanese, C., Santoru, A., Emmler, T., et al. (2019). A New Mutually Destabilized Reactive Hydride System: $\text{LiBH}_4\text{-Mg}_2\text{NiH}_4$. *J. Energ. Chem.* 34, 240–254. doi:10.1016/j.jechem.2019.03.011
- Bilen, M., Yilmaz, O., and Gürü, M. (2015). Synthesis of LiBH_4 from LiBO_2 as Hydrogen Carrier and its Catalytic Dehydrogenation. *Int. J. Hydrogen Energ.* 40 (44), 15213–15217. doi:10.1016/j.ijhydene.2015.02.085
- Choi, Y. J., Lu, J., Sohn, H. Y., Fang, Z. Z., Kim, C., Bowman, R. C., et al. (2011a). Reaction Mechanisms in the $\text{Li}_3\text{AlH}_6/\text{LiBH}_4$ and Al/LiBH_4 Systems for Reversible Hydrogen Storage. Part 2: Solid-State NMR Studies. *J. Phys. Chem. C* 115 (13), 6048–6056. doi:10.1021/jp109113f
- Choi, Y. J., Lu, J., Sohn, H. Y., and Fang, Z. Z. (2011b). Reaction Mechanisms in the $\text{Li}_3\text{AlH}_6/\text{LiBH}_4$ and Al/LiBH_4 Systems for Reversible Hydrogen Storage. Part 1: H Capacity and Role of Al. *J. Phys. Chem. C* 115 (13), 6040–6047. doi:10.1021/jp109112t
- Dematteis, E. M., Dematteis, E. R., Roedern, E., Pinatel, E. R., Corno, M., Jensen, T. R., et al. (2016). A Thermodynamic Investigation of the $\text{LiBH}_4\text{-NaBH}_4$ System. *RSC Adv.* 6, 60101–60108. doi:10.1039/c6ra09301a
- Ding, Z., Lu, Y., Li, L., and Shaw, L. (2019). High Reversible Capacity Hydrogen Storage through Nano- LiBH_4 + Nano- MgH_2 System. *Energ. Storage Mater.* 20, 24–35. doi:10.1016/j.ensm.2019.04.025
- Ding, Z., Wu, P., and Shaw, L. (2019). Solid-state Hydrogen Desorption of 2 MgH_2 + LiBH_4 Nano-Mixture: A Kinetics Mechanism Study. *J. Alloys Comp.* 806, 350–360. doi:10.1016/j.jallcom.2019.07.218
- Guo, Y. H., Yu, X. B., Gao, L., Xia, G. L., Guo, Z. P., and Liu, H. K. (2010). Significantly Improved Dehydrogenation of LiBH_4 destabilized by TiF_3 . *Energy Environ. Sci.* 3 (4), 465–470. doi:10.1039/b915779d
- Halim Yap, F. A., and Ismail, M. (2018). Functions of MgH_2 in the Hydrogen Storage Properties of a $\text{Na}_3\text{AlH}_6\text{-LiBH}_4$ Composite. *J. Phys. Chem. C* 122 (42), 23959–23967. doi:10.1021/acs.jpcc.8b07934
- Halim Yap, F. A., Mustafa, N. S., Yahya, M. S., Mohamad, A. A., and Ismail, M. (2018). A Study on the Hydrogen Storage Properties and Reaction Mechanism of $\text{Na}_3\text{AlH}_6\text{LiBH}_4$ Composite System. *Int. J. Hydrogen Energ.* 43 (17), 8365–8374. doi:10.1016/j.ijhydene.2018.03.070
- Hansen, B. R. S., Ravnsbæk, D. B., Reed, D., Book, D., Gundlach, C., Skibsted, J., et al. (2013). Hydrogen Storage Capacity Loss in a $\text{LiBH}_4\text{-Al}$ Composite. *J. Phys. Chem. C* 117 (15), 7423–7432. doi:10.1021/jp312480h
- Ismail, M., Zhao, Y., Yu, X. B., and Dou, S. X. (2012). Improved Hydrogen Storage Performance of $\text{MgH}_2\text{-NaAlH}_4$ Composite by Addition of TiF_3 . *Int. J. Hydrogen Energ.* 37 (10), 8395–8401. doi:10.1016/j.ijhydene.2012.02.117
- Jain, I. P., Jain, P., and Jain, A. (2010). Novel Hydrogen Storage Materials: A Review of Lightweight Complex Hydrides. *J. Alloys Comp.* 503 (2), 303–339. doi:10.1016/j.jallcom.2010.04.250
- Jiang, K., Xiao, X., Chen, L., Han, L., Li, S., Ge, H., et al. (2012). A Comparative Study of the Hydrogen Storage Properties of LiBH_4 Doping with CaHCl and CaH_2 . *J. Alloys Comp.* 539, 103–107. doi:10.1016/j.jallcom.2012.06.039
- Langmi, H. W., McGrady, G. S., Newhouse, R., and Rönnebro, E. (2012). $\text{Mg}_2\text{FeH}_6\text{-LiBH}_4$ and $\text{Mg}_2\text{FeH}_6\text{-LiNH}_2$ Composite Materials for Hydrogen Storage. *Int. J. Hydrogen Energ.* 37 (8), 6694–6699. doi:10.1016/j.ijhydene.2012.01.020
- Li, G., Matsuo, M., Deledda, S., Sato, R., Hauback, B. O. R. C., and Orimo, S.-i. (2013). Dehydrogenation Property of LiBH_4 Combined with Mg_2FeH_6 . *Mater. Trans.* 54 (8), 1532–1534. doi:10.2320/matertrans.M2013145
- Li, Y., Li, P., and Qu, X. (2017). Investigation on $\text{LiBH}_4\text{-CaH}_2$ Composite and its Potential for Thermal Energy Storage. *Sci. Rep.* 7, 41754. doi:10.1038/srep41754
- Li, Y., Wu, S., Zhu, D., He, J., Xiao, X., and Chen, L. (2020). Dehydrogenation Performances of Different Al Source Composite Systems of $2\text{LiBH}_4 + \text{M}$ ($\text{M} = \text{Al}, \text{LiAlH}_4, \text{Li}_3\text{AlH}_6$). *Front. Chem.* 8, 227. doi:10.3389/fchem.2020.00227
- Li, Y., Xiao, X., Chen, L., Han, L., Shao, J., Fan, X., et al. (2012). Effects of Fluoride Additives on the Hydrogen Storage Performance of $2\text{LiBH}_4\text{-Li}_3\text{AlH}_6$ Destabilized System. *J. Phys. Chem. C* 116 (42), 22226–22230. doi:10.1021/jp307572x
- Lin, W., Xiao, X., Wang, X., Wong, J.-W., Yao, Z., Chen, M., et al. (2020). Extreme High Reversible Capacity with over 8.0 Wt% and Excellent Hydrogen Storage Properties of MgH_2 Combined with LiBH_4 and Li_3AlH_6 . *J. Energ. Chem.* 50, 296–306. doi:10.1016/j.jechem.2020.03.076
- Liu, D. M., Tan, Q. J., Gao, C., Sun, T., and Li, Y. T. (2015). Reversible Hydrogen Storage Properties of LiBH_4 Combined with Hydrogenated $\text{Mg}_{11}\text{CeNi}$ Alloy. *Int. J. Hydrogen Energ.* 40 (20), 6600–6605. doi:10.1016/j.ijhydene.2015.03.130
- Liu, H., Wang, X., Zhou, H., Gao, S., Ge, H., Li, S., et al. (2016). Improved Hydrogen Desorption Properties of LiBH_4 by AlH_3 Addition. *Int. J. Hydrogen Energ.* 41 (47), 22118–22127. doi:10.1016/j.ijhydene.2016.09.177
- Liu, S.-S., Zhang, Y., Sun, L.-X., Zhang, J., Zhao, J.-N., Xu, F., et al. (2010). The Dehydrogenation Performance and Reaction Mechanisms of Li_3AlH_6 with TiF_3 Additive. *Int. J. Hydrogen Energ.* 35 (10), 4554–4561. doi:10.1016/j.ijhydene.2009.12.108
- Liu, X.-S., Liu, H.-Z., Qiu, N., Zhang, Y.-B., Zhao, G.-Y., Xu, L., et al. (2021). Cycling Hydrogen Desorption Properties and Microstructures of $\text{MgH}_2\text{-AlH}_3\text{-NbF}_5$ Hydrogen Storage Materials. *Rare Met.* 40, 1003–1007. doi:10.1007/s12598-020-01425-1
- Ma, Y., Li, Y., Liu, T., Zhao, X., Zhang, L., Han, S., et al. (2016). Enhanced Hydrogen Storage Properties of LiBH_4 Generated Using a Porous Li_3BO_3 Catalyst. *J. Alloys Comp.* 689, 187–191. doi:10.1016/j.jallcom.2016.07.313
- Mao, J. F., Guo, Z. P., Liu, H. K., and Yu, X. B. (2009a). Reversible Hydrogen Storage in Titanium-Catalyzed $\text{LiAlH}_4\text{-LiBH}_4$ System. *J. Alloys Comp.* 487 (1–2), 434–438. doi:10.1016/j.jallcom.2009.07.158
- Mao, J. F., Yu, X. B., Guo, Z. P., Poh, C. K., Liu, H. K., Wu, Z., et al. (2009b). Improvement of the $\text{LiAlH}_4\text{-NaBH}_4$ System for Reversible Hydrogen Storage. *J. Phys. Chem. C* 113 (24), 10813–10818. doi:10.1021/jp808269v
- Mao, J., Guo, Z., Leng, H., Wu, Z., Guo, Y., Yu, X., et al. (2010). Reversible Hydrogen Storage in Destabilized $\text{LiAlH}_4\text{-MgH}_2\text{-LiBH}_4$ Ternary-Hydride System Doped with TiF_3 . *J. Phys. Chem. C* 114 (26), 11643–11649. doi:10.1021/jp1012208
- Mao, J., Guo, Z., Yu, X., Ismail, M., and Liu, H. (2011). Enhanced Hydrogen Storage Performance of $\text{LiAlH}_4\text{-MgH}_2\text{-TiF}_3$ Composite. *Int. J. Hydrogen Energ.* 36 (9), 5369–5374. doi:10.1016/j.ijhydene.2011.02.001
- Mao, J., Guo, Z., Yu, X., and Liu, H. (2013). Combined Effects of Hydrogen Back-Pressure and NbF_5 Addition on the Dehydrogenation and Rehydrogenation Kinetics of the $\text{LiBH}_4\text{-MgH}_2$ Composite System. *Int. J. Hydrogen Energ.* 38 (9), 3650–3660. doi:10.1016/j.ijhydene.2012.12.106
- Meethom, S., Kaewsuan, D., Chanlek, N., Utke, O., and Utke, R. (2020). Enhanced Hydrogen Sorption of $\text{LiBH}_4\text{-LiAlH}_4$ by Quenching Dehydrogenation, Ball Milling, and Doping with MWCNTs . *J. Phys. Chem. Sol.* 136, 109202. doi:10.1016/j.jpccs.2019.109202
- Mustafa, N. S., Halim Yap, F. A., Yahya, M. S., and Ismail, M. (2018). The Hydrogen Storage Properties and Reaction Mechanism of the $\text{NaAlH}_4 + \text{Ca}(\text{BH}_4)_2$ Composite System. *Int. J. Hydrogen Energ.* 43 (24), 11132–11140. doi:10.1016/j.ijhydene.2018.04.234
- Mustafa, N. S., and Ismail, M. (2019). Significant Effect of TiF_3 on the Performance of $2\text{NaAlH}_4 + \text{Ca}(\text{BH}_4)_2$ Hydrogen Storage Properties. *Int. J. Hydrogen Energ.* 44 (39), 21979–21987. doi:10.1016/j.ijhydene.2019.06.080
- Puszkiewicz, J., Gennari, F. C., Arneodo Larochette, P., Troiani, H. E., Karimi, F., Pistidda, C., et al. (2014). Hydrogen Storage in Mg-LiBH_4 Composites Catalyzed by FeF_3 . *J. Power Sourc.* 267, 799–811. doi:10.1016/j.jpowsour.2014.05.130
- Sofianos, M. V., Sheppard, D. A., Rowles, M. R., Humphries, T. D., Liu, S., and Buckley, C. E. (2017). Novel Synthesis of Porous Mg Scaffold as a Reactive Containment Vessel for LiBH_4 . *RSC Adv.* 7, 36340–36350. doi:10.1039/C7RA05275H
- Sofianos, M. V., Sheppard, D. A., Silvester, D. S., Lee, J., Paskevicius, M., Humphries, T. D., et al. (2018). Electrochemical Synthesis of Highly Ordered Porous Al Scaffolds Melt-Infiltrated with LiBH_4 for Hydrogen Storage. *J. Electrochem. Soc.* 165 (2), D37–D42. doi:10.1149/2.0481802jes
- Soru, S., Taras, A., Pistidda, C., Milanese, C., Bonatto Minella, C., Masolo, E., et al. (2014). Structural Evolution upon Decomposition of the $\text{LiAlH}_4 + \text{LiBH}_4$ System. *J. Alloys Comp.* 615, S693–S697. doi:10.1016/j.jallcom.2013.12.027
- Surrey, A., Bonatto Minella, C., Fechner, N., Antonietti, M., Grafe, H.-J., Schultz, L., et al. (2016). Improved Hydrogen Storage Properties of LiBH_4 via Nanoconfinement in Micro- and Mesoporous Aerogel-like Carbon. *Int. J. Hydrogen Energ.* 41 (12), 5540–5548. doi:10.1016/j.ijhydene.2016.01.163

- Thaweelap, N., and Utke, R. (2016). Dehydrogenation Kinetics and Reversibility of LiAlH₄-LiBH₄ Doped with Ti-Based Additives and MWCNT. *J. Phys. Chem. Sol.* 98, 149–155. doi:10.1016/j.jpccs.2016.07.005
- Tu, G., Xiao, X., Jiang, Y., Qin, T., Li, S., Ge, H., et al. (2015). Composite Cooperative Enhancement on the Hydrogen Desorption Kinetics of LiBH₄ by Co-doping with NbCl₅ and Hexagonal BN. *Int. J. Hydrogen Energ.* 40 (33), 10527–10535. doi:10.1016/j.ijhydene.2015.06.168
- Wu, X., Wang, X., Cao, G., Li, S., Ge, H., Chen, L., et al. (2012). Hydrogen Storage Properties of LiBH₄-Li₃AlH₆ Composites. *J. Alloys Comp.* 517, 127–131. doi:10.1016/j.jallcom.2011.12.054
- Xia, G.-l., Leng, H.-y., Xu, N.-x., Li, Z.-l., Wu, Z., Du, J.-l., et al. (2011). Enhanced Hydrogen Storage Properties of LiBH₄-MgH₂ Composite by the Catalytic Effect of MoCl₃. *Int. J. Hydrogen Energ.* 36 (12), 7128–7135. doi:10.1016/j.ijhydene.2011.03.060
- Xiang, M., Zhang, Y., Zhu, Y., Guo, X., Chen, J., and Li, L. (2018). Ternary LiBH₄-NaBH₄-MgH₂ Composite as Fast Ionic Conductor. *Solid State Ionics* 324, 109–113. doi:10.1016/j.ssi.2018.06.015
- Yahya, M. S., Ali, N. A., Sazelee, N. A., Mustafa, N. S., Halim Yap, F. A., and Ismail, M. (2019). Intensive Investigation on Hydrogen Storage Properties and Reaction Mechanism of the NaBH₄-Li₃AlH₆ Destabilized System. *Int. J. Hydrogen Energ.* 44 (39), 21965–21978. doi:10.1016/j.ijhydene.2019.06.076
- Yang, Y., Gao, M., Liu, Y., Wang, J., Gu, J., Pan, H., et al. (2012). Multi-hydride Systems with Enhanced Hydrogen Storage Properties Derived from Mg(BH₄)₂ and LiAlH₄. *Int. J. Hydrogen Energ.* 37 (14), 10733–10742. doi:10.1016/j.ijhydene.2012.04.068
- Yu, X. B., Guo, Y. H., Sun, D. L., Yang, Z. X., Ranjbar, A., Guo, Z. P., et al. (2010). A Combined Hydrogen Storage System of Mg(BH₄)₂-LiNH₂ with Favorable Dehydrogenation. *J. Phys. Chem. C* 114 (10), 4733–4737. doi:10.1021/jp910547s
- Zang, L., Sun, W., Liu, S., Huang, Y., Yuan, H., Tao, Z., et al. (2018). Enhanced Hydrogen Storage Properties and Reversibility of LiBH₄ Confined in Two-Dimensional Ti₃C₂. *ACS Appl. Mater. Inter.* 10 (23), 19598–19604. doi:10.1021/acsami.8b02327
- Zhang, Y., Liu, Y., Yang, Y., Li, Y., Hu, J., Gao, M., et al. (2018). Superior Catalytic Activity of In Situ Reduced Metallic Co for Hydrogen Storage in a Co(OH)₂-containing LiBH₄/2LiNH₂ Composite. *Mater. Res. Bull.* 97, 544–552. doi:10.1016/j.materresbull.2017.09.037
- Zhao, Y., Jiao, L., Liu, Y., Guo, L., Li, L., Liu, H., et al. (2014). A Synergistic Effect between Nanoconfinement of Carbon Aerogels and Catalysis of CoNiB Nanoparticles on Dehydrogenation of LiBH₄. *Int. J. Hydrogen Energ.* 39 (2), 917–926. doi:10.1016/j.ijhydene.2013.10.137
- Zheng, J., Yao, Z., Xiao, X., Wang, X., He, J., Chen, M., et al. (2021). Enhanced Hydrogen Storage Properties of High-Loading Nanoconfined LiBH₄-Mg(BH₄)₂ Composites with Porous Hollow Carbon Nanospheres. *Int. J. Hydrogen Energ.* 46, 852–864. doi:10.1016/j.ijhydene.2020.09.177
- Zhou, H., Wang, X., Liu, H., and Yan, M. (2017). Enhanced Hydrogen Storage Properties of 2LiBH₄-LiAlH₄ Nanoconfined in Resorcinol Formaldehyde Carbon Aerogel. *J. Alloys Comp.* 726, 525–531. doi:10.1016/j.jallcom.2017.07.080
- Züttel, A., Rentsch, S., Fischer, P., Wenger, P., Sudan, P., Mauron, P., et al. (2003). Hydrogen Storage Properties of LiBH₄. *J. Alloys Comp.* 356-357, 515–520. doi:10.1016/s0925-8388(02)01253-7

Conflict of Interest: The authors declare that the research was conducted in the absence of any commercial or financial relationships that could be construed as a potential conflict of interest.

Copyright © 2021 Li, Zhang and Chen. This is an open-access article distributed under the terms of the Creative Commons Attribution License (CC BY). The use, distribution or reproduction in other forums is permitted, provided the original author(s) and the copyright owner(s) are credited and that the original publication in this journal is cited, in accordance with accepted academic practice. No use, distribution or reproduction is permitted which does not comply with these terms.